LABORATORY INVESTIGATION

Mechanism of anti-glioma activity and in vivo efficacy of the cannabinoid ligand KM-233

Steven N. Gurley · Ammaar H. Abidi · Patrick Allison · Peihong Guan ·
Christopher Duntsch · Jon H. Robertson · Stanley D. Kosanke · Stephen T. Keir ·
Darell D. Bigner · Andrea J. Elberger · Bob M. Moore II

Abstract Glioblastoma multiforme (GBM) is the most common and devastating form of primary central nervous system malignancy. The prognosis for patients diagnosed with GBM is poor, having a median survival rate of 12–15 months. Despite modern advances in the development of antineoplastic agents, the efficacy of newer anti-cancer agents in the treatment of GBM is yet to be determined. Thus, there remains a significant unmet need for new therapeutic strategies against GBM. A promising chemotherapeutic intervention has emerged from studies of cannabinoid receptor agonists wherein tetrahydrocannabinol has been the most extensively studied. The novel cannabinoid ligand KM-233 was developed as a lead platform for future optimization of biopharmaceutical properties of classical based cannabinoid ligands. Treatment of U87MG human GBM cells with KM-233 caused a time dependent change in the phosphorylation profiles of MEK, ERK1/2, Akt, BAD, STAT3, and p70S6K. Almost complete mitochondrial depolarization was observed 6 h post-treatment followed by a rapid increase in cleaved caspase 3 and significant cytoskeletal contractions. Treatment with KM-233 also resulted in a redistribution of the Golgi-endoplasmic reticulum structures. Dose escalation studies in the orthotopic model using U87MG cells revealed an 80 % reduction in tumor size after 12 mg/kg daily dosing for 20 days. The evaluation of KM-233 against primary tumor tissue in the side flank model revealed a significant decrease in the rate of tumor growth. These findings indicate that structural refinement of KM-233 to improve its biopharmaceutical properties may lead to a novel and efficacious treatment for GBM.

S. N. Gurley · A. H. Abidi · P. Allison · P. Guan ·
B. M. Moore II (✉)
Department of Pharmaceutical Sciences, The University
of Tennessee Health Science Center, Memphis, TN, USA
e-mail: bmoore@uthsc.edu

C. Duntsch · J. H. Robertson
Department of Neurosurgery, The University of Tennessee
Health Science Center, Memphis, TN, USA

S. D. Kosanke
Department of Pathology, University of Oklahoma Health
Sciences Center, Oklahoma City, OK, USA

S. T. Keir
Department of Surgery, Duke University, Durham, NC, USA

D. D. Bigner
Department of Pathology, Duke University, Durham, NC, USA

A. J. Elberger
Department of Anatomy and Neurobiology, The University
of Tennessee Health Science Center, Memphis, TN, USA

Introduction

Brain malignancies are the second and fifth leading causes of cancer-related deaths in males and females ages 20–39, respectively [1]. The most prevalent form of adult primary central nervous system (CNS) tumors is collectively referred to as glioma, and the most common, devastating, and high-grade glioma is glioblastoma multiforme (GBM) [1, 2]. These tumors are classically thought to originate from supporting or glial cells of the CNS, and represent roughly 50 % of all adult primary CNS tumors. Long term survival of patients with a GBM diagnosis with the best radiotherapeutic, surgical, and anti-tumor drug therapy available is extremely rare. Specifically, the median

survival for GBM patients is 12–15 months depending on age and other prognostic factors [3]. It is therefore essential that new therapeutic interventions for this devastating disease be identified and developed.

The endocannabinoid system has emerged as one of the most promising targets for the development of novel chemotherapy agents for the treatment of GBM [4, 5]. The interest in cannabinoids as anti-GBM agents began with the reported cytotoxicity of Δ^9-tetrahydrocannabinol (THC) against rat C6.9 glioma cells [6]. The discovery of anti-GBM activity of THC catalyzed research into the therapeutic potential of THC, and other cannabinoid (CB) ligands, for the treatment of GBM [7–14]. By far, THC has been the most systematically studied CB ligand with respect to cell death biochemical cascades and in vivo activity [15–21], and was used in a small clinical trial of efficacy in GBM patients [22]. The mechanism of CB action has received considerable attention with respect to signaling cascades and receptor subtype contributions. There is strong support for a mechanism wherein THC triggers autophagy and cell death via an eIF2a-p8-Akt-mTROC1 pathway [19]. Autophagy in U87MG cells is inhibited by co-administration of the CB1 selective antagonist/inverse agonist SR141716, thus suggesting a CB1 mediated pathway. Primary tissue samples are reported to express both the CB1 and CB2 receptors with an intriguing bias for the CB2 receptor in GBM [23]. In a comparison of GBM, meningioma, and astrocytoma, the GBM manifested a significant decrease in CB1 immunoreactivity relative to controls, meningioma, and astrocytoma [24].

We have developed and previously tested the novel cannabinoid ligand KM-233 in the side flank model of GBM [7]. These results prompted us to conduct a more detailed evaluation of KM-233. The first objective was to compare the effect(s) of KM-233 to the published effect(s) of THC on U87MG GBM cells [19]. The activity of KM-233 is blocked by the CB1 receptor antagonist SR141716A but not the CB2 antagonist WIN55,212-3. We have now found that treatment of U87MG cells with KM-233 significantly alters protein phosphorylation, caspase 3 activation, cytochrome C (cyt C) release, and the endoplasmic reticulum structure. In addition, systematic administration of KM-233 significantly reduced tumor size in the U87MG orthotopic model of GBM and delayed tumor growth in flank models using newly diagnosed GBM tumor tissue.

Materials and methods

Cell culture and in vitro cytotoxicity assays

The human GBM cell line U87MG (American Type Culture Collection, ATCC, Manassas, VA) was maintained in Eagle's Minimum Essential Medium (EMEM) supplemented with 10 % FBS and pen/strep at 37 °C in an atmosphere of 5 % CO_2/95 % air until needed for cytotoxicity pathway assays. For cytotoxicity assays cells were plated in 96-well polystyrene flat-bottom plates (7,500 cells/well) at 70 % confluence in a 100 µl total volume of supplemented media as indicated, and incubated overnight at 37 °C to allow for adherence. The EMEM was then replaced with EMEM containing 1 % FBS and the cultures were inoculated with escalating amounts of drug ranging from 0.3 to 100 µM; cell death was analyzed at 18 h using the BioTek Synergy 2 Multidetection Microplate Reader (BioTek Instruments, Inc. Winooski, VT). Cytoxicity assays aimed at identifying the target receptor were carried out as above with the addition of 10 and 20 µM SR141716A (selective CB1 antagonist) or WIN-55,212-3 (neutral antagonist CB2 receptor). The percentage of viable cells present in the culture at each time point was calculated by comparing the absorbance value at 450 nm using the CCK-8 assay (Dojindo Molecular Technologies, Rockville, MD) for each condition with untreated control cells. All assays were conducted per manufacturer's protocol. All described values represent the average of three data points per determination and three independent determinations.

In vivo studies utilized a U87MG glioma cell line that was previously stably transduced with the pFB retrovirus (pFB-GFP) (Stratagene, La Jolla, CA) expressing green fluorescent protein (GFP) to enhance visual analysis. The cells were grown in Dulbecco's Modified Eagle Medium (DMEM) supplemented with 10 % FBS, 1× non-essential amino acids (NEAA) and 0.01 M HEPES buffer. U87MG-GFP cells in exponential growth were harvested with EDTA/trypsin for 5 min at 37 °C. The cells were centrifuged for 5 min at 1,000 RPM, and the pellets were resuspended in sterile 10 µl PBS at a concentration of 1×10^5 cells per sample and placed on ice until implantation.

Phospho-protein quantification and apoptosis analysis using Meso Scale Discovery (MSD) MULTI-ARRAY® microplate technology

U87MG cells were plated in poly-D-lysine coated 10 cm Petri dishes at a density of 4×10^5 cells/ml with 12 ml of cell suspension added to each plate. The cells were grown overnight in EMEM media containing 10 % FBS. The following day the media was changed to EMEM media containing 1 % FBS and allowed to equilibrate for 24 h. This step is essential to allow basal levels of signaling proteins to re-equilibrate due to changes in the serum concentration. The media was then replaced at the appropriate time points with media containing 1 % serum and KM-233 at the EC_{50} concentration or media containing

1 % serum and vehicle (DMSO). After the incubation period with KM-233, the media was removed from the dishes and transferred to a 15 ml centrifuge tube to collect any cells that were in suspension. Cells were then scraped from the surface of the dish and transferred into the same 15 ml centrifuge tubes and pelleted at 1,000 RPM, 4 °C for 5 min. Supernatant was removed and 0.5 ml lysis buffer was added to each pellet. The cells were suspended in the buffer and transferred to 1.5 ml microcentrifuge tubes. These were incubated on ice for 30 min, while being vortexed every 5 min. The lysates were then centrifuged at $10,000 \times g$, 4 °C for 10 min to clear cellular debris from the lysate. The supernatant was removed and assayed for protein concentration using a Pierce BCA Protein Assay Kit (Thermo Scientific). The lysates were then diluted with complete lysis buffer to a concentration of 20 µg of protein in 25 µl volume. Signaling proteins were then analyzed using MSD phosphoprotein and intracellular marker multiplex kits which were imaged on a SECTOR Imager 2400 according to the manufacturer's instructions. The following kits were used for analysis; cleaved caspase-3, pp53 (Ser 15), PARP human apoptosis whole cell lysate kit; pERK1/2 (Thr/Tyr: 202/204; 185/187), pJNK (Thr 183/Tyr 185), pp38 (Thr 180/Tyr 182) human MAP kinase whole cell lysate kit; pAkt (Ser 473), pGSK-3β (Ser 9), pp70S6K (Thr 421/Ser 424) human Akt signaling whole cell lysate kit; ERK1/2 (Thr/Tyr: 202/204; 185/187), MEK1/2 (Ser 217/221), STAT3 (Tyr 705) human ERK-STAT3 cascade whole cell lysate kit; pBAD plate; and total BAD plate.

Mitochondrial membrane potential assay

U87MG cells were cultured and drug-treated as described for Meso Scale Discovery (MSD) MULTI-ARRAY® microplate analysis using black well poly-D-lysine plates. The time intervals for the study were 0, 1, 3, 6 and 8 h drug exposure. The DePsipher™ kit for the Detection of Mitochondrial Membrane Potential (cat. #6300-100-K, Trevigen, Inc, Gaithersburg, MD) was used to evaluate the status of mitochondrial membrane polarization. DePsipher is a lipophilic cation that aggregates when the membrane is polarized to form a red fluorescent compound. If polarization is interfered with, the dye remains/reverts to a green fluorescent compound. The Incubation solution was prepared, containing 1× Reaction Buffer, Stabilizer Solution, and the DePsipher solution. Media was removed and cells were treated with Incubation solution for 15 min in a humidified incubator with 5 % CO_2 in air at 37 °C, then incubation solution was removed and replaced with Reaction Buffer. Cells were immediately examined on a Zeiss 710 with 34-Channel Spectral Detection confocal laser scanning microscope. A 488 nm laser line imaged the green label, and a 561 nm laser line imaged the red label.

Multi-parameter cell death

Cells were seeded in 10 % FBS EMEM at 10,000–20,000 per well in Biocoat collagen I 96-well plates, and then incubated at 37 °C for 24 h. A Multiparameter Cell Death Kit (Cellomics #8408002, Thermo Fisher Scientific, Pittsburgh, PA) was used. It contained DAPI, a Cell Permeability Dye, and primary antibodies to cyt C and LC3B for detection of apoptosis and autophagy, respectively. LC3B is expressed as distinct spots in the cytoplasm, and cyt C is released from the mitochondria so that it is distributed through the cytoplasm and the nucleus; these events occur prior to nuclear condensation, increased cell permeability, and cell loss. The EC_{50} concentration of KM-233, prepared in 1 % EMEM, was used. A mixture of 1 µl KM-233 and 100 µl 37 °C 1 % serum media was used to obtain the desired concentration for cell exposure. Media with FBS was removed, and replaced with the KM-233/1 % serum media mixture. Drug treatment durations were 1, 3, 6, 12 and 18 h. Control wells with 1 % serum media and DMSO were included with each assay. The 'Positive Control' represents baseline staining for the U87MG cells treated with the drug MG132 (the control drug used by the kit manufacturer) and treatment durations were 6 and 18 h. After the treatment cycle was completed, cells were fixed for 15 min with 4 % paraformaldehyde, which was added after the removal of the cell media. Cells were imaged with a Zeiss LSM710 laser scanning confocal microscope, using the 405 nm laser line for DAPI, the 488 nm laser line for the Cell Permeability Dye, the 561 laser line for the cyt C, and the 633 nm laser line for the LC3B. However, the LC3B antibody proved to be weak and faded quickly, therefore transmission electron microscopy was utilized to view autophagy ultrastructurally.

Note: since the time course studies were conducted on single plates, the addition of the drugs was reversed, i.e. 18 h back to 1 h such that all samples were fixed simultaneously, to prevent potential complicating effects of paraformaldehyde from adjacent wells.

Organelle lights assay

U87MG cells were plated on collagen coated 96 well plates at the density of 10,000 cells per well and equilibrated for 24 h. The Cellular Lights™ human Golgi-resident enzyme N acetylgalactosaminyltransferase 2-GFP tagged and al-reticulin and KDEL (ER retention signal)-RFP tagged vectors in the BacMam expression system (Invitrogen, Carlsbad, CA) were used to label the target organelles according to the manufacturer's recommendations. 200 µl of these cocktails were added to each well, incubated for 4 h with gentle hand mixing at 15 min intervals. After the incubation time, the cocktail was replaced with 0 % serum

EMEM media and enhancer solution per manufacturer's protocol. This solution was incubated for 2 h, then replaced with 10 % serum EMEM media and then cultured for 24 h. Expression of GFP and RFP was verified by epifluorescence microscopy and then the time course was initiated by drug treatment as described for Meso Scale Discovery (MSD) MULTI-ARRAY® microplate analysis. At the predetermined time points of 1, 3, 6, and 9 h, as well as positive and vehicle controls, cells were fixed in 4 % paraformaldehyde solution for 15 min, washed twice with DPBS, and then the nuclear stain DAPI was introduced for 20 min. After washing, samples were stored in 150 μL of DPBS in sealed plates protected from light prior to analysis. Cells were imaged using a Zeiss LSM710 laser scanning confocal microscope, using the 405 nm laser line for DAPI, the 488 nm laser line for the GFP, and the 561 laser line for the RFP.

Note: since the time course studies were conducted on single plates, the addition of the drugs was reversed, i.e. 9 h back to 1 h such that all samples were fixed simultaneously, to prevent potential complicating effects of paraformaldehyde from adjacent wells.

Transmission electron microscopy

U87MG cells were cultured and drug-treated as described for Meso Scale Discovery (MSD) MULTI-ARRAY® microplate analysis with the exception of trypsin treatment to remove the cells rather than scraping. The time intervals for the drug treatment were 2, 4, 6, and 8 h as well as vehicle control at 8 h. The cells were pelleted, fixed in 2 % glutaraldehyde in PBS for 2 h, post-fixed in 1 % osmium tetroxide in PBS for 4 h, rinsed briefly in deionized water, and *en bloc* stained with 2 % uranyl acetate in 0.85 % sodium chloride overnight at 4° C. The slices were dehydrated in graded solutions of alcohol, from 30–100 % at 1 h each, infiltrated first with 50 % Spurr resin in 100 % alcohol overnight at room temperature, then 100 % Spurr over a 24 h period involving at least 4 changes of Spurr. They were cured at 60° C for 2 days. The pellets were sectioned at approximately 75 nm on a Reichert Ultracut E microtome, and post-stained with uranyl acetate and lead citrate. The tissue was observed and photographed on a JEOL 2000EX TEM at 60 kV.

Orthotopic model of human GBM using U87MG cells

Adult male CB-17 SCID mice, 25–35 g in weight, were used for all studies and handled in accordance with protocols approved by the Institutional Animal Care and Use Committee at the University of Tennessee Health Science Center. Animals were anesthetized with an intraperitoneal injection of ketamine 87 mg/kg, and xylazine 13 mg/kg body weight, and placed in a stereotaxic frame. The hair was removed along the midline of the skull and the area disinfected with betadine. An incision approximately 5 mm in length was made at the midline to locate the sagittal and coronal sutures. A small burr hole was made with a handheld drill 3 mm lateral from the midline along the bregma suture over the right hemisphere. Utilizing a sterile Hamilton syringe, 1×10^5 U87MG cells stably expressing GFP (see *Cell culture and* in vitro *cytotoxicity assays*) in 10 μl sterile PBS (prepared as described above) was injected over a period of 2 min at a depth of 2 mm from the brain surface. The scalp defect was then closed with 4.0 vicryl sutures. Mice were observed daily for signs of infection, alertness, feeding habits, and neurological deficits related to tumor growth. The tumors were unimpeded for 5 days, and mice were then randomly assigned to one of 6 treatment cohorts ($n = 10$ per cohort) and subjected to a control and dose escalation study. The cohorts in the study consisted of: (1) no treatment; (2) 100 μl of vehicle; 3) 100 μl at a KM-233 dose of 2 mg/kg; 4) 100 μl at a KM-233 dose of 4 mg/kg; 5) 100 μl at a KM-233 dose of 8 mg/kg; and 6) 100 μl at a KM-233 dose of 12 mg/kg. Doses were injected i.p. twice daily. The dosing regimen was selected based on the 4 to 12 h duration of psychotropic effects associated with oral THC administration [25]. The vehicle for KM-233 consisted of 100 μl of saline containing 3 % cremophor and 3 % ethanol. Mice were euthanized at 25 days after tumor inoculation or earlier if any evidence of a significant neurological deficit, pain or discomfort, was noted. Under deep anesthesia, the mice were euthanized by transcardial perfusion with 4 % paraformaldehyde. The brains were coronally sectioned on a vibratome at 40 μm thickness and prepared for epifluorescence confocal laser scanning microscopy using a Bio-Rad MRC 1024. The pancreas, spleen, liver, lungs, thymus, kidney, heart, and intestines from the treatment cohorts were subjected to histopathologic analysis to assess for potential toxicity. At the end of the study, the following cohort numbers survived the course of the experiments: 1) control $n = 9$; 2) vehicle control $n = 9$; 3) 2 mg/kg $n = 7$; 4) 4 mg/kg $n = 8$; 5) 8 mg/kg $n = 8$; and 6) 12 mg/kg $n = 9$.

Flank model of human GBM using primary tumor tissues

Male and female athymic mice (nu/nu genotype, Balb/c background, 6–8 weeks old) were used for all antitumor studies. Animals were maintained in filter top cages in Thoren units (Thoren Caging Systems, Inc., Hazelton, PA). All animal procedures conformed to Duke University Institutional Animal Care and Use Committee and National Institute of Health guidelines.

The following patient-derived human glioblastoma multiforme xenografts maintained at the Preston Robert Tisch Brain Tumor Center at Duke: D-08-0673 MG and D-09-0362

MG, were used for subcutaneous (sc) studies. In preparation for sc transplantation, sc xenografts passaged in athymic mice were excised from host mice under sterile conditions in a laminar flow containment hood. The xenograft was processed through a modified tissue press to create a homogenate. The resulting homogenate was then loaded into a repeating Hamilton syringe dispenser. Tumor homogenate was injected sc into the right flank of the athymic mouse at an inoculation volume of 50 μl with a 19 gauge needle [26]. Subcutaneous tumors were measured twice weekly with hand-held vernier calipers (Scientific Products, McGraw, IL). Tumor volumes, V were calculated with the following formula: $[(\text{width})^2 \times (\text{length})]/2 = V \text{ (mm}^3)$.

For the sc tumor studies, groups of mice randomly selected by tumor volume were treated when the median tumor volumes were on average 100–300 mm^3 and were compared with control animals receiving either KM233 or vehicle control.

Statistical analysis

Meso Scale Discovery (MSD) MULTI-ARRAY® microplate analyses were performed using three biological replicates assayed in duplicate. Changes in phospho-protein and caspase 3 levels relative to time 0 were evaluated by Student's t test, p value were subjected to a Bonferroni correction with statistical significance defined as 0.001, i.e. 0.05/48 p values. Orthotopic GBM model data were evaluated by a one-way ANOVA of the untreated control versus all treatments and vehicle control versus drug treatment. The response of sc xenografts to treatment was assessed by delay in tumor growth and by tumor regression. Growth delay, expressed as T-C, is defined as the difference in days between the median time required for tumors in treated (T) and control (C) animals to reach a volume five times greater than that measured at the start of the treatment. Tumor regression is defined as a decrease in tumor volume over two successive measurements. Statistical analyses were performed using a SAS statistical analysis program, the Wilcoxon rank order test for growth delay, and Fisher's exact test for tumor regression as previously described [27, 28].

Results

CB1 and CB2 component of KM-233 activity

The KM series of classical cannabinoids [10] incorporates an aryl or heteroaryl group at the C1' position as illustrated in Fig. 1. This modification yields a group of analogs that generally exhibit modest selectivity for the CB2 over the CB1 receptor. To further assess the target of KM-233 at the CB1 and CB2 receptors, cytotoxicity assays were
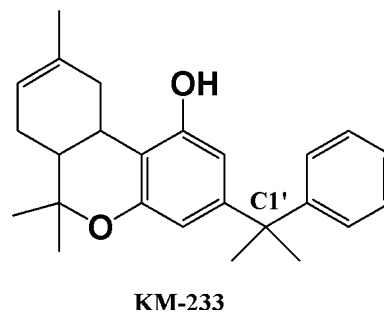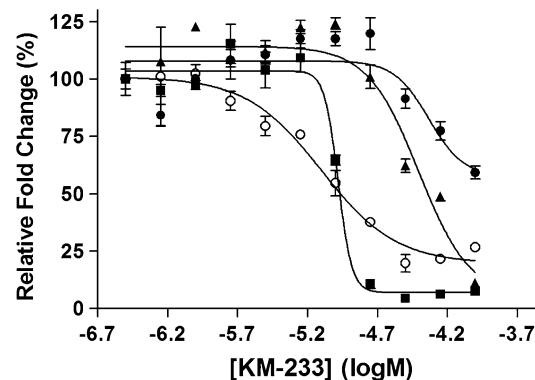

Fig. 1 Chemical structure of KM-233

Fig. 2 Evaluation of the cytotoxicity of KM-233 in the absence and presence of SR141716A (CB1 antagonist) and WIN-55,212-3 (CB2 antagonist). KM-233 dose response curves *filled squares*, KM-233 plus 10 μM SR141716A *filled triangles*, KM-233 plus 10 μM SR141716A *filled circles*, and KM-233 plus 10 μM WIN-55,212–3 *open circles*

conducted in the absence and presence of the CB1 antagonist SR141716A and CB2 neutral antagonist WIN-55,212-3. Co-administration of 10 μM M SR141716A in the assays yielded a dextral shift in the curve that appeared to manifest surmountable antagonism (Fig. 2). To test surmountable antagonism the assay was repeated using 20 μM yielding an increased dextral shift thus indicating the CB1 receptor component of KM-233 activity. Blockade of the CB2 receptor using WIN55,212-3 failed to inhibit activity of KM-233 against U87MG cells. These results are consistent with the earlier report that the activity of THC against U87MG is inhibited by SR141716A [19].

Analysis of apoptosis markers and phospho-protein profiles of KM-233 treated U87MG cells

The biological pathways affected by treatment of U87MG cells with THC have been reported. Therefore, we conducted experiments to gain insight into the mechanism of cell death and allow comparison of the effects of KM-233 to those previously reported for THC. The structure of KM-233 is unique and allows for chemical modification to improve the biopharmaceutical properties, however, prior to
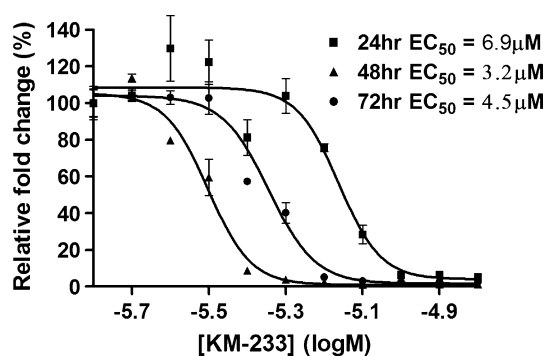
Fig. 3 Cytotoxicity of KM-233 against U87MG cells analyzed as a function of exposure time

extensive chemical efforts it is critical to understand and validate the mechanism(s) of cell death. We first determined the in vitro cytotoxicity of KM-233 as a function of exposure time to establish the parameter for subsequent analysis of apoptosis markers and phospho-protein profiles. Treatment of U87MG cells with increasing concentrations of KM-233 (0.3 to 100 μM) for 24, 48, and 72 h revealed a small but significant decrease in EC_{50} with increased exposure times (Fig. 3). The 48 and 72 h treatments, however, resulted in cells that readily detached from the plate; this was deemed unacceptable for the immunofluorescence studies. Therefore, the 24 h interval was selected for subsequent evaluation of the effects of KM-233 on U87MG cells. The second phase in pre-experimental development was to determine the time window in which the levels of cellular apoptotic markers increase, thus identifying the start of non-specific cell death cascades. To this end, U87MG cells were treated with KM-233 at the EC_{50} concentration and analyzed at 0, 1, 6, 12, 18, and 24 h for cleaved caspase-3, pp53, and cleaved PARP levels using Meso Scale Discovery (MSD) MULTI-ARRAY® microplate technology. The MSD technology was selected in place of Western blots since it provides significant advantages in terms of speed and quantitation [29, 30]. The time intervals were selected as a first approximation of when, on the time course from treatment to death, significant changes in early and late biochemical markers could be detected. Of these 3 apoptotic markers, only cleaved caspase-3 manifested a significant increase in the 24 h interval reaching a maximum at 18 h post-treatment (Fig. 4).

The evaluation of cell signaling cascade(s) preceding caspase-3 cleavage focused first on the classic cell fate regulating protein kinase pathways ERK1/2, JNK, and p38. Over the 0, 1, 6, 12, 18, and 24 h drug treatment time course only pERK exhibited a significant change in relative levels in response to drug treatment. Thus, these results restricted our evaluation of the classic pathways to ERK1/2 as well as pathway related kinases MEK1/2 and STAT3, using the MSD multiplex assay. A significant increase in pSTAT3 occurred 1 h post-drug treatment, increased by a
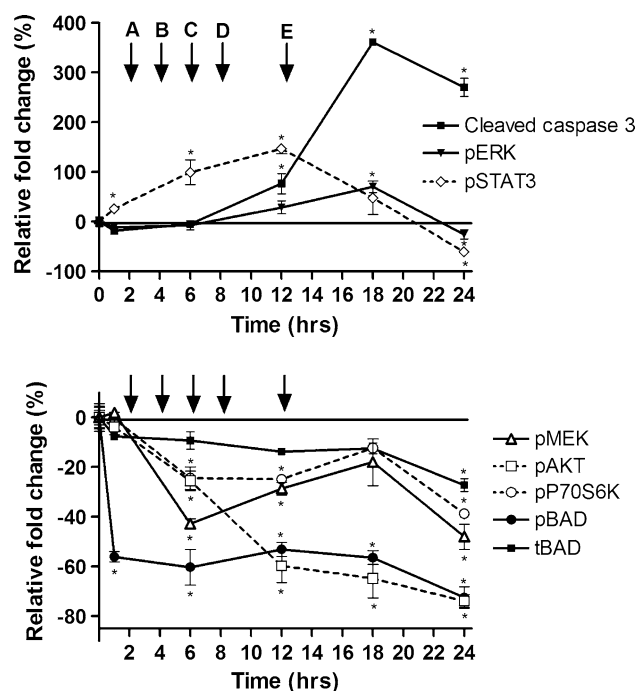

Fig. 4 Phospho-protein and cleaved caspase 3 profiles of U87MG cells treated with KM-233 for the designated time intervals. The *upper panel* presents proteins manifesting positive changes and the *lower panel* negative changes. *Arrows* mark observed significant morphological events that were consistent with changes in phospho-protein and cleaved caspase 3 levels. *A*: By 2 h, early evidence of mitochondrial changes in TEM was observed (Fig. 8). *B*: By 4 h mitochondria manifested partial depolarization, and evidence of Golgi-RER dysfunction were observed (Figs. 5, 7). *C*: By 6 h, mitochondria were completely depolarized, cyt C release was initiated, and TEM analysis revealed significant mitochondrial swelling (Figs. 5, 6, and 8). *D*: By 8 h, extensive RER swelling was observed in the TEM images (Fig. 8). *E*: By 12 h extensive release of cyt C was observed (Fig. 6). Statistical significance defined as $p < 0.001$ (*) was based on a Bonferroni correction of multiple p values calculated by the Student's t test

relative 180 % at 12 h, then rapidly declined at 24 h (Fig. 4). pERK1/2 remained near basal level through 6 h followed by a significant increase in phosphorylation through 18 h and a final decline at 24 h. In contrast, the pMEK level significantly declined by 25 % at 6 h post-drug exposure. This trend transiently reversed at 18 h, although not reaching basal levels and then declined again at 24 h (Fig. 4). Interestingly, the consistent decline in phospho-protein levels at 24 h may reflect prolonged activation (6 h) of caspase-3.

The IP3K-Akt axis is a critical pro-survival mechanism in many human cancers including glioma and U87MG cells [31, 32]. Analysis of the effect(s) of KM-233 on this cascade was accomplished using the pAkt, pGSK3b, pP70S6K multiplex MSD plate. Treatment of U87MG cells with KM-233 caused a significant and rapid decrease in pAkt that first manifested at 6 h (Fig. 4). The decrease in pAkt was paralleled by a concomitant decrease in pP70S6K at

6 h. We further utilized the MSD technology to assess a mitochondrial contribution to cell death by analyzing the effects of KM-233 on total and pBAD. A contribution of the mitochondria to cell death was investigated based on a potential mitochondria- cyt C-caspase 3 mediated pathway. Exposure of cells to KM-233 did not affect the total BAD levels 1 h post-exposure exhibiting a small but insignificant decrease over the remaining time course (Fig. 4). However, a significant decrease in pBAD occurred at 1 h and persisted through the 24 h experimental window (Fig. 4). Interestingly, pBAD decline did not correlate with reductions in pAkt or pERK, thus raising the possibility that an unidentified protein phosphatase is regulated by the drug; i.e. based on the relatively rapid rate of pBAD loss.

The temporal changes in critical pro- and anti-apoptotic proteins were expected to manifest effects on U87MG organelle structure and function. For example, upstream activation of caspase-3 mediated through mitochondrial cyt C release correlates directly with loss of mitochondrial function. The loss of mitochondrial function, as determined by the membrane polarization ($\Delta\psi_m$), was evaluated as a marker for the potential onset of cyt C release. Treatment of U87MG cells with KM-233 resulted in a significant decrease in $\Delta\psi_m$ as indicated by the inability of the fluorescent stain dePsipher® to form red eximers inside mitochondria at 3 h, and an almost complete depolarization at 6 h (Fig. 5). Confirmation of cyt C release was accomplished using the Cellomics multiparameter cell death kit to assess cyt C, LC3B, and cell membrane permeability (Fig. 6). At 0 h, the U87MG cells manifest a normal mitochondrial network appearance. Evidence of drug effects first manifest at 3 h, with some cells showing increased focal concentrations of cyt C. At 6 h, there is a significant uptake of whole cell permeability stain; furthermore, the cyt C label reveals disruption of the mitochondrial network. Specifically, the mitochondrial network has collapsed into dense clusters of cyt C labeling around and colocalizing with the nucleus, suggestive of cyt C release (Fig. 6). Extensive cyt C release and significant loss of cell membrane potential occurs 12 h post-treatment which progressed throughout the remainder of the 24 h time course. However, we were unable to detect LC3B immunostaining; although, LC3 activation has been previously demonstrated in autophagic cell death in U87MG cells treated with THC [19].

Notwithstanding, the role of autophagy in THC-induced U87MG cell death is documented and warranted further examination. Since ER stress can be a precipitating event in the autophagic process, we selected the Organelle Lights assay system to monitor the ER-Golgi response(s) to KM-233. The assay uses human Golgi-resident enzyme *N*-acetylgalactosaminyltransferase 2-GFP tagged and alreticulin and KDEL (ER retention signal)-RFP tagged vectors in the BacMam expression system to label the Golgi and ER, respectively. U87MG expressing both GFP and RFP labels were treated with KM-233 and the intracellular locations of the tags was monitored by confocal laser scanning microscopy. Beginning at 3 h, there was a colocalization of the RFP and GFP labels which intensified at 6 h suggesting a convergence of the ER and Golgi structures. At 9 h, the labeling was similar to that of the positive control, staurosporine, which is an inducer of ER stress (Fig. 7). The colocalization of the tags indicates that the ER-Golgi membranes are either in close proximity or merged. Light microscopy does not permit a definitive interpretation of the results; therefore, an ultrastructural examination of organelle structural responses to KM-233 treatment was conducted.

The time course of the transmission electron microscope (TEM) studies was refined to reflect the early decrease in pBAD and the significant changes in protein phosphorylation patterns occurring through 12 h. It was predicted that there would be a time lag between pBAD decline and mitochondria effects. Therefore, the time intervals examined were condensed to 2, 4, 6, and 8 h as well as vehicle control at 8 h. Time points past 8 h were not considered since any organelle insult should manifest prior to this based on the significant increase of cleaved caspase 3 after 12 h. In alignment with biochemical and light microscopic data, U87MG cells exposed to KM-233 revealed a progressive series of morphological changes consistent with temporally-linked changes previously observed. The mitochondria in KM-233 treated U87MG manifested a progressive derangement in morphology consistent with the dePsipher® and cyt C studies. Specifically, 2 h post-treatment a spectrum of mitochondrial structures was detected ranging from normal, to vesicular-swollen (VS), to swollen (S) morphology (Fig. 8) [33]. At 6 h, the predominant morphologies were VS and S, consistent with extensive mitochondrial dysfunction. At 6 h, swelling of the rough endoplasmic reticulum (RER) was observed. Another feature observed was the emergence of autophagosomes and autophagic compartments at 4 h (Fig. 9). These compartments appear to contain VS mitochondria as well as laminar structures with indistinct morphology. At 6 h post-treatment, autophagic vesicles appeared to contain Golgi-ER structures as suggested by the presence of ribosomes and multi-laminar structures. The co-occurance of these structures, suggesting an autophagic process, is consistent with the co-localization of the fluorescent probes in the Organelle Lights study. These data are consistent with the reported autophagic cell death in THC-treated U87MG cells [19]. The 8 h time interval is characterized by extensive mitochondrial and pronounced RER swelling (Fig. 8). The combined data from our studies indicates that KM-233 initiates cell death via the intrinsic death pathway with subsequent activation of autophagic processes.
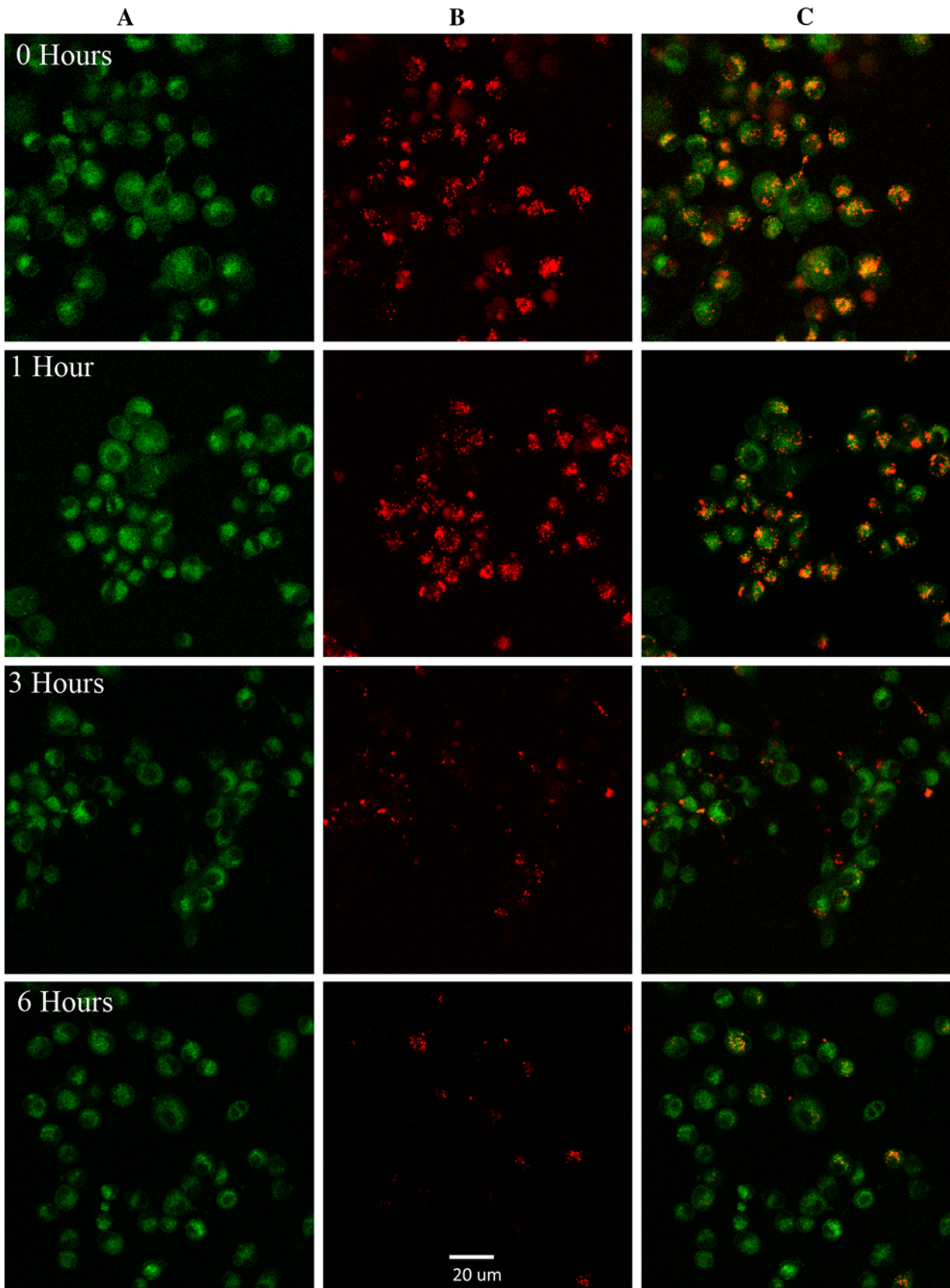
Fig. 5 Results of the dePsipher® membrane depolarizer kit. The kit labels appear as follows: the dePsipher cation is *green* (column **A** images) and when the membrane is polarized ($\Delta\psi_m$), it aggregates and appears *red* (column **B** images), but when membrane polarity is abnormal, the aggregation is disrupted and the cation is only seen as *green*; merged images are presented in column **C**. At 0 h, the U87MG membrane potential is normal and the cation has aggregated so that it displays matching images when viewed with the 561 and 488 nm laser lines. With KM-233 at 1 h, there is a significant decrease in $\Delta\psi_m$ as signified by the reduced conversion to the *red* aggregated form. The loss of mitochondrial function is determined by $\Delta\psi_m$. At 3 h, there is a further depolarization as demonstrated by the reduced *red* form. By 6 h, with KM-233 there is almost complete depolarization as indicated by the inability of the dePsipher® to exhibit the *red* form

In vivo efficacy of KM-233 in the orthotopic GBM model

The ability of KM-233 to initiate a rapid onset of events leading to apoptosis raises the question of whether this activity would translate into in vivo efficacy. To address this question, KM-233 was evaluated in the orthotopic model of human GBM using U87MG cells. Tumors were induced in SCID mice by direct intracranial inoculation of human GFP-expressing U87MG cells. A 5 day growth period was allowed, and then the animals were assigned randomly to treatment groups of intraperitoneal injection twice a day for 20 subsequent days with vehicle, 2, 4, 8, or 12 mg/kg of KM-233. At the end of the 25 day experimental window, the effect of KM-233 on tumor surface area was evaluated. A general dose response was observed across treatment groups with significant reductions in tumor area manifesting at 8 and 12 mg/kg doses (Fig. 10). At the dose of 12 mg/kg, an 80 % reduction in tumor volume was observed. Micrographs of the 2 control cohorts manifest a diffuse pattern of GFP expressing U87MG cells compared to relatively well demarcated labeling in the 8 and 12 mg/kg doses (Fig. 11). The pancreas, spleen, liver, lungs, thymus, kidney, heart, and intestines from the
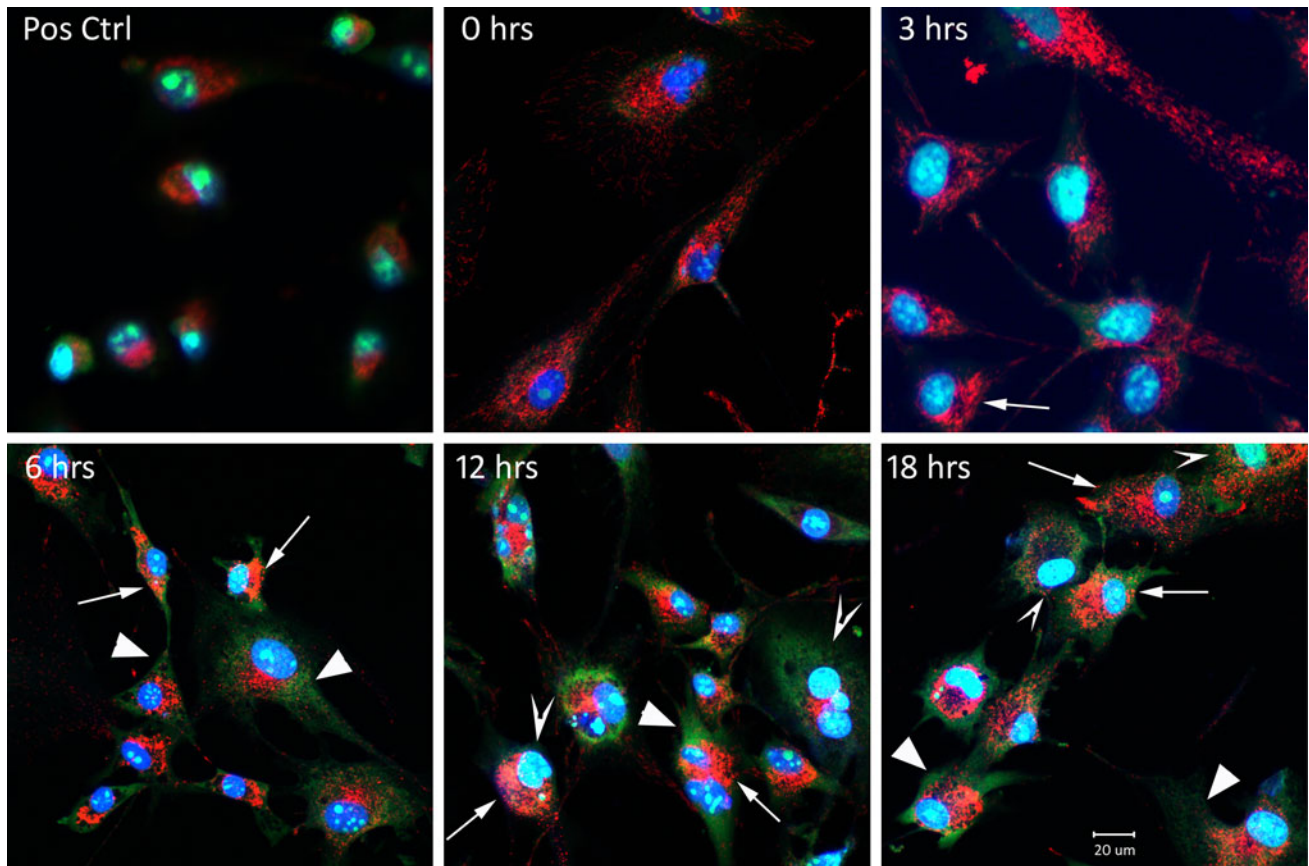

Fig. 6 Results of multiparameter cell death kit. Images of U87MG cells treated with KM-233 at 0, 3, 6, 12, and 18 h, along with the positive control of U87MG cells treated with the drug MG132 at 6 h, are demonstrated. The kit labels appear as follows: cell nuclei with DAPI (*blue*), whole cell permeability stain (*green*), and cytochrome C (*red*). At 3 h, the normal mitochondrial network appearance begins to reveal changes in terms of focal concentrations of cyt C (*arrow*). At 6 h, the cell membrane has become permeabilized as observed in the distribution of *green* label through the cytoplasm (*arrowheads*). Also at 6 h, the collapse of the mitochondrial network has caused the cyt C to become densely clustered over and around the nucleus (*arrows*). At 12 h, further permeabilization of membranes appears to have occurred, as indicated by the migration of the whole cell dye into the nucleus; the *green* label combined with the *blue* DAPI gives a 'seafoam green' appearance (*chevrons*). These changes in the *red* and *green* labels have progressed further at 24 h
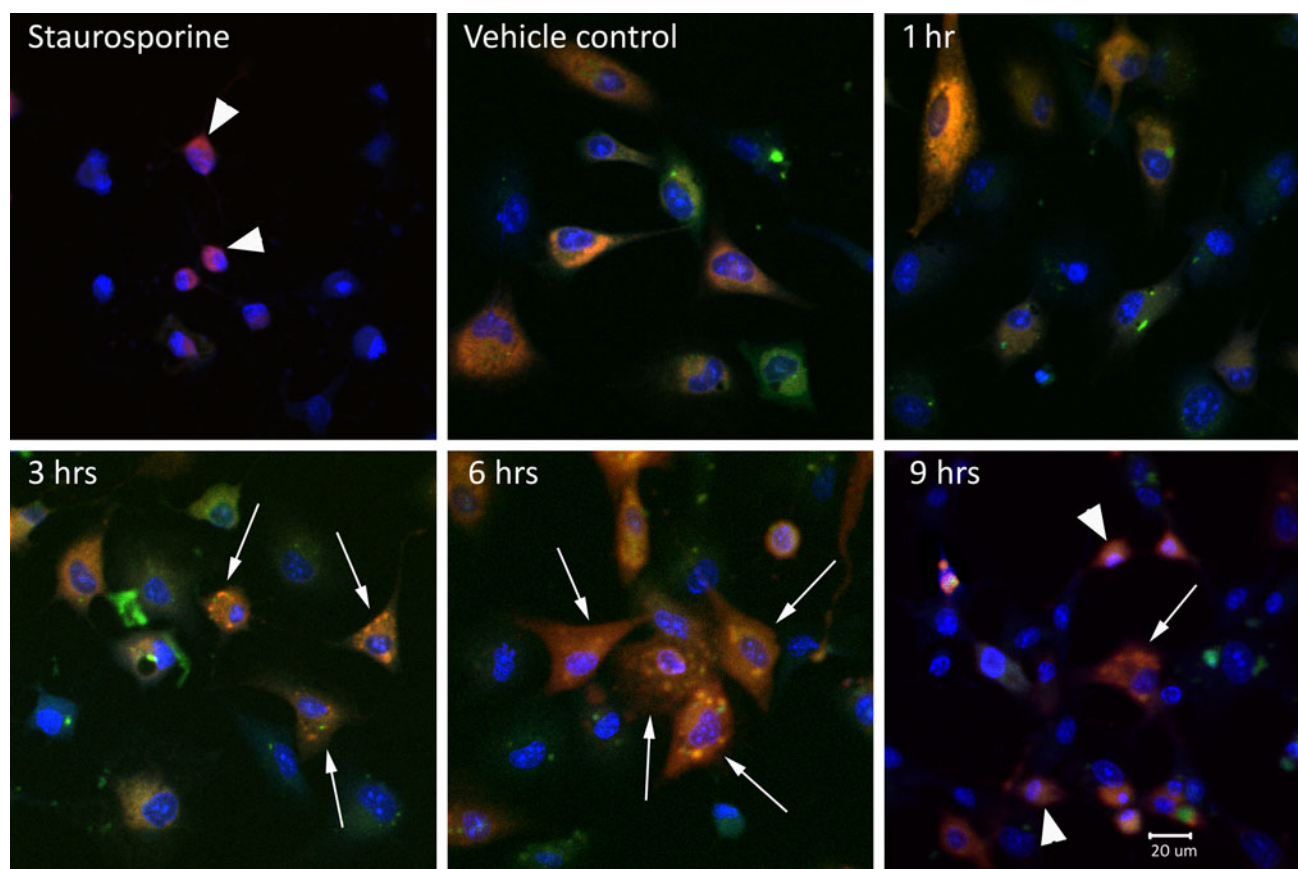
Fig. 7 Results of the organelle lights assay system. Images of U87MG cells treated with KM-233 at 1, 3, 6, 9 h, along with a vehicle control, and a positive control of U87MG cells with staurosporine at 2 h are demonstrated. The labels appear as follows: DAPI nuclear stain (*blue*), Golgi-resident enzyme *N*-acetylgalactosaminyltransferase 2-GFP (*green*), alreticulin ER retention signal and KDEL-RFP (*red*). Beginning at 3 h, the punctate GFP and RFP labels show colocalization suggesting the merging of the ER and Golgi structures (*arrows*). There is increased colocalization (*arrows*) at 6 h. By 9 h, the cells resemble those of the ER stress inducer staurosporine (*arrowheads*), with little colocalization (*arrow*)

treatment cohorts were subjected to histopathologic analysis to assess for potential toxicity. None of these organs revealed any definitive evidence of toxicity-related tissue damage related to KM-233 administration. This included the absence of acute tissue necrosis/apoptosis, acute inflammation or increased mitotic activity. These studies, in conjunction with the flank model reported earlier [7], suggest that KM-233 is safe and effective in reducing tumor load, even in the context of the blood brain barrier, and even when given systemically.

In vivo efficacy of KM-233 in the flank model using primary human GBM samples

The U87MG models system is widely used for preliminary assessment of the efficacy of novel compounds against GBM. While an effective screening tool, the model does not recapitulate many aspects of human primary tumors [34]. To better assess the future potential of KM-233 against GBM, a study was conducted utilizing primary GBM cells (D-08-0673 MG and D-09-0362 MG) derived from newly diagnosed patients. Tumors were inoculated in the flank of nu/nu genotype, Balb/c mice and animals were randomly assigned to control and KM-233 treatment cohorts. Animals were dosed twice daily with 12 mg/kg KM-233 or vehicle control and tumor size evaluated as function of time. Treatment with KM-233 provided a significant growth delay, expressed as T-C, defined as the difference in days between the median time required for tumors in treated (T) and control (C) animals to reach a volume five times greater than that measured at the start of treatment (Figs. 12, 13).

Discussion

The urgent need for new therapeutic interventions against GBM is unquestionable and requires the identification of new targets for systematic drug design efforts. Two emerging targets for the development of novel anti-GBM

Fig. 8 TEM micrographs of U87MG cells treated with KM-233. Cells treated with vehicle manifest normal organelle and mitochondrial morphology (*white arrows*). At 2 h post-treatment, a spectrum of mitochondrial morphologies was observed that include normal (*white arrow*), vesicular-swollen (VS) (*chevrons*); and swollen (S) structures (*black arrows*). At 6 h, the majority of mitochondria are in the swollen form (*black arrows*) and the RER manifests early swelling. Extensive swelling of the RER is observed at 8 h with continued degradation of mitochondria. The original magnification was 20,000× and the *scale bar* represents 500 nm
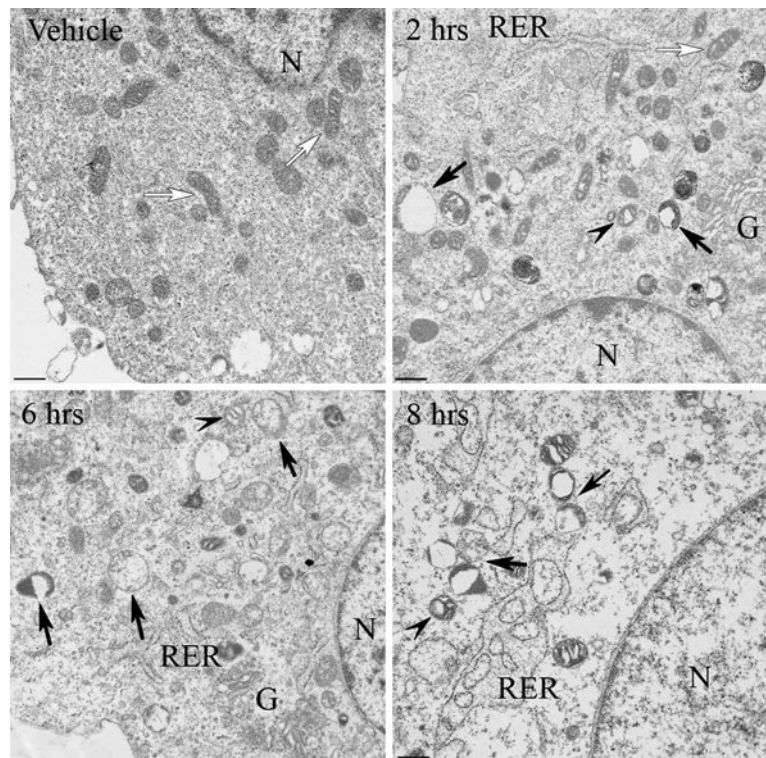

Fig. 9 TEM micrographs of U87MG cells treated with KM-233. **A**, **B**, and **C** represent the 4 h time interval wherein autophagic compartments are first detected. **A** The double–double walled structure (*chevron*) is indicative of an autophagic compartment, possibly containing a VS mitochondrion. This interpretation is based on the structure of VS mitochondria present in **B**. **C** An autophagic compartment (*chevron*) manifests laminar structures of indeterminate origin. **D** At 6 h, an autophagic compartment containing ribosomes and multi-laminar structures is detected. This compartment may arise from dysfunction of the Golgi-ER. The original magnification was 50,000× and the *scale bar* represents 500 nm
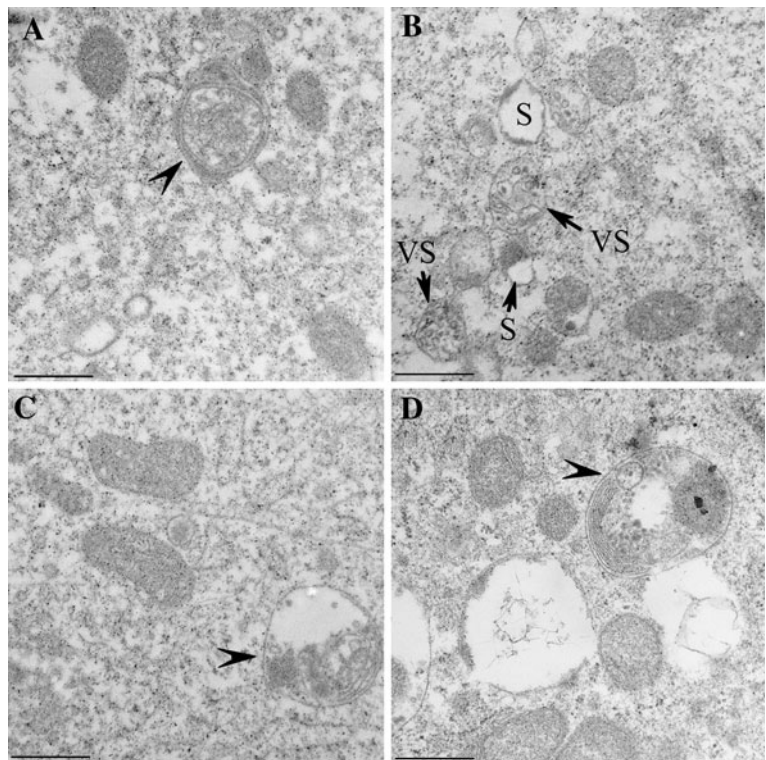
agents are the CB1 and CB2 receptors. In order to effectively exploit the receptor system, it is critical to understand the receptor subtype selective requirements of CB receptor ligands. We first confirmed the receptor contribution to the in vitro cytotoxicity of KM-233. The selective CB1 receptor antagonist SR141716A blocked activity of KM-233 while the CB2 receptor antagonist WIN-55,212-3 had no effect. This result is consistent with the previous report of SR141716A inhibiting the cytotoxicity of THC against U87MG cells.
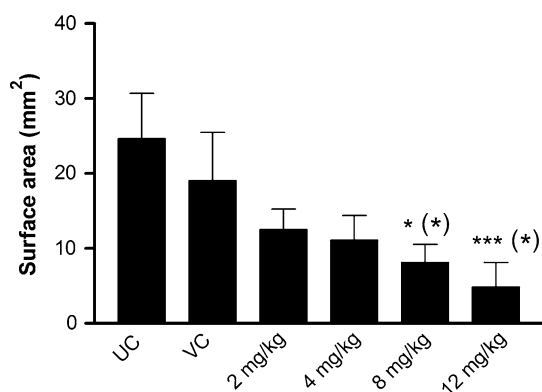
Fig. 10 Tumor load in the U87MG orthotopic glioma model in SCID mice. Cohorts consisted of untreated control (UC), vehicle control (VC), and escalating doses of KM-233 administered twice daily for 20 days. A one-way ANOVA of the UC versus all treatments (*symbols without parenthesis*) and VC versus drug treatment (*symbols with parenthesis*) was conducted. * $p < 0.05$ and *** $p < 0.001$

Fig. 12 Tumor volume in the flank model using D-08-0673 MG. The control cohort is illustrated using *filled squares* and the KM-233 treated cohort using *filled triangles*

We have previously reported the in vivo efficacy of KM-233 in the side flank model of human GBM [7], which prompted us to investigate the pathways involved in KM-233 anti-GBM activity in more detail. The in vitro studies highlighted temporal changes in biochemical markers and cellular morphology in KM-233 treated U87MG glioma cells. Interestingly, the two major execution programs in apoptosis, i.e. the caspase pathway and organelle 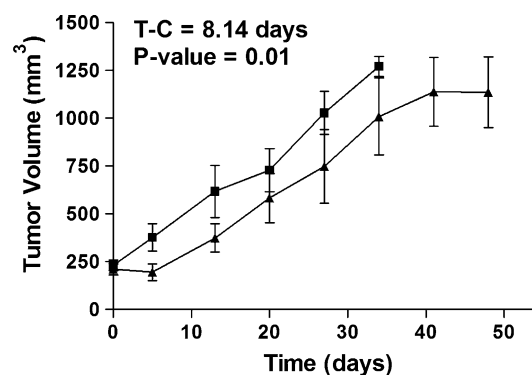dysfunction [35, 36], are observed in our studies. One hour post-treatment, there is a significant decrease in pBAD. Dephosphorylation of BAD triggers translocation to the mitochondria, and inactivation of BCL-xL and BCL2, resulting in a sequellae of pro-apoptotic events initiated at the mitochondrial level. Although cannabinoids have been shown to activate BAD in C6 glioma cells, colorectal cancer cell lines and Jurkat leukemia T cells, the inhibition was regulated upstream by Akt and ERK [37–39]. While our data cannot exclude these pathways, i.e. insignificant change in pAKT and pERK at 1 h, the absence of reduced phosphorylation levels is inconsistent with the rapid decrease in pBAD.
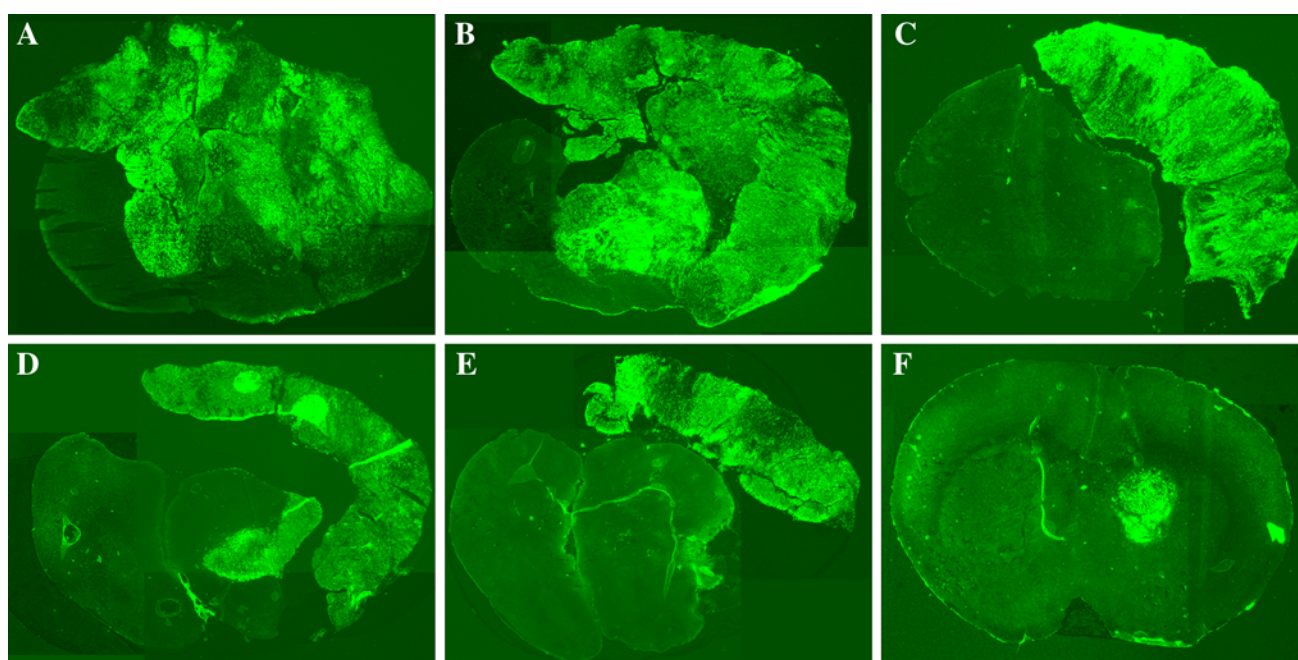

Fig. 11 Representative fluorescence photomicrographs showing tumor sizes in mouse brains where: **A** untreated control **B** vehicle control; **C** 2 mg/kg KM-233; **D** 4 mg/kg KM-233; **E** 8 mg/kg KM-233; and **F** 12 mg/kg KM-233. Brains were serial sectioned and pictures represent the largest fluorescent section within an animal brain where measurements were taken
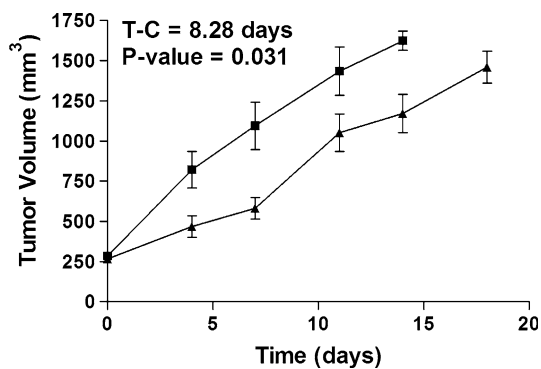
Fig. 13 Tumor volume in the flank model using D-09-0362 MG. The control cohort is illustrated using *filled squares* and the KM-233 treated cohort using *filled triangles*

The significant decrease in pBAD was expected to be accompanied by alterations in mitochondrial function; therefore, we conducted experiments to examine the integrity of mitochondria in KM-233 cells. Evidence of early mitochondrial swelling in the EM studies was followed by a detectable decrease in Ψ_m after a 3 h exposure to KM-233. The effect of KM-233 on mitochondrial integrity was clearly defined as evidenced by the pronounced mitochondrial swelling observed in the TEM studies at 4 h. Within this time interval a release of cyt C is detected which is expected and consistent with the loss of Ψ_m after a 3 h exposure to KM-233. Combined, these findings are consistent with the observed upstream reduction in pBAD that may result in the subsequent inhibition of the anti-apoptotic BCL-xL and BCL2 proteins. The transition into the 6 h data set was marked by the formation of autophagic compartments and vacuoles as diagnostic of autophagy and, in combination with mitochondrial dysfunction, suggests the start of a mitochondria-mediated initiation of autophagy. The initiation of autophagy is consistent with earlier reports; however, the underlying mechanism wherein THC initiates autophagy was via an ER stress mediated mechanism [19].

In the aforementioned study, THC initiated autophagy in U87MG cells via an upstream Akt-mTOR mediated autophagic pathway as in U87MG cells [19]. To test this contribution we examined the levels of pAkt and P70S6K, down-stream mediator of mTOR, in U87MG cells treated with KM-233. The time dependent decrease in pAkt and P70S6K levels is consistent with the results using THC. Furthermore, the Organelle Lights study and transmission electron microscopy support a potential mechanism involving ER stress. The major differences between our study and the previous report is the timing, mitochondrial dysfunction, cyt C release, and caspase 3 activation proceeding evidence of autophagy. Autophagy can represent a pro-survival response to organelle dysfunction and thus is

reversible in this scenario. However, it is not possible to determine if the autophagic process is reversible, and thus non-lethal, due to the initiation of the caspase 3 death pathway at 12 h.

It has previously been suggested that cannabinoids are an unlikely therapeutic intervention in glioma unless Akt is inactived in conjunction with ERK [40]. The current study reveals that KM-233 significantly reduces pAkt and has no effect on pERK1/2 until 12 h post-treatment. The increase in pERK1/2 occurs in the same time interval as caspase 3 activation; therefore, the significance of the increase relative to survival is an open question. Notwithstanding, the impact on pAkt levels observed for U87MG cells is potentially an important criteria to be considered in the development of KM-233. The unusual increase in pSTAT, relative to the general trend of the other phospho-proteins, suggests that this pathway is an important survival pathway in U87MG glioma, which has been reported in various glioma cultures [41–43]. Interestingly enough, however, is that KM-233 effectively overrides this pathway since the ultimate outcome is cell death. The use of cannabinoid based anti-GBM agents may represent an indirect approach to overcoming survival mechanisms associated with STAT3 activation. [44]

We next examined if the promising in vitro activity translated into in vivo efficacy in the orthotopic model of human GBM using U87MG cells. A dose escalation study of KM-233 from 2 to 12 mg/kg twice daily i.p. injections was conducted to determine the efficacy of the drug delivered via systemic administration, i.e. penetration of the blood brain barrier. At doses of 8 and 12 mg/kg, statistically significant 68 and 80 % reductions in tumor area relative to control and vehicle control were observed with no evidence of acute organ toxicity associated with twice daily KM-233 dosing up to 12 mg/kg. The U87MG model system is widely used to screen potential drug candidates; however, a comparative examination of U87MG in orthotopic models reveals that it does not manifest critical attributes of human tumors [34]. To better assess the efficacy of KM-233, we examined the in vivo efficacy in the flank model using primary human GBM tissue. Administration of 12 mg/kg KM-233 in this model yielded a statistically significant increase in the T-C in both models demonstrating growth reduction in primary tumors. This is the first evidence that KM-233 is effective against primary human GBM tissue. Further studies will be required to determine if KM-233, or a related analog, can be optimized to improve the in vivo activity against GBM.

The combined in vivo and in vitro pharmacology data presented herein indicate that KM-233 mechanisms of anti-GBM action are distinct from those reported for other classical cannabinoids such as THC. The convergence of potentially two death cascades, i.e. the intrinsic pathway

and autophagic pathway, is predicted to aid in preventing drug resistance associated with the single mechanism of action drugs. The data also provide a foundation for the future development of newer KM-233 analogs with improved biopharmaceutical properties. In summary, the unique activity of cannabinoid based ligands against GBM provides a novel approach for the future development of clinically relevant anti-GBM agents.

Conflict of interest The authors declare that they have no conflict of interest.

References

1. Jemal A, Siegel R, Ward E, Hao Y, Xu Z, Thun TJ (2009) Cancer statistics, 2009. Cancer J Clin 59:225–249
2. Surawicz TS, Davis F, Freels S, Laws ER Jr, Menck HR (1998) Brain tumor survival: results from the National Cancer Data Base. J Neurooncol 40(2):151–160
3. Van Meir EG, Hadjipanayis CG, Norden AD, Shu HK, Wen PY, Olson JJ (2010) Exciting new advances in neuro-oncology: the avenue to a cure for Malignant Glioma. Cancer J Clin 60:166–193
4. Parolaro D, Massi P (2008) Cannabinoids as potential new therapy for the treatment of gliomas. Expert Rev Neurother 8:37–49
5. Velasco G, Carracedo A, Blázquez C, Lorente M, Aguado T, Haro A, Sánchez C, Galve-Roperh I, Guzmán M (2007) Cannabinoids and gliomas. Mol Neurobiol 36:60–67
6. Sanchez C, Galve-Roperh I, Canova C, Brachet P, Guzman M (1998) Delta9-tetrahydrocannabinol induces apoptosis in C6 glioma cells. FEBS Lett 436(1):6–10
7. Duntsch C, Divi MK, Jones T, Zhou Q, Krishnamurthy M, Boehm P, Wood G, Sills A, Moore BM (2006) Safety and efficacy of a novel cannabinoid chemotherapeutic, KM-233, for the treatment of high-grade glioma. J Neurooncol 77:143–152
8. Galve-Roperh I, Rueda D, Gómez dPT, Velasco G, Guzmán M (2002) Mechanism of extracellular signal-regulated kinase activation by the CB(1) cannabinoid receptor. Mol Pharmacol 62:1385–1392
9. Jacobsson SO, Wallin T, Fowler CJ (2001) Inhibition of rat C6 glioma cell proliferation by endogenous and synthetic cannabinoids. Relative involvement of cannabinoid and vanilloid receptors. J Pharmacol Exp Ther 299(3):951–959
10. Krishnamurthy M, Gurley S, Moore BM (2008) Exploring the substituent effects on a novel series of C1′-dimethyl-aryl Delta8-tetrahydrocannabinol analogs. Bioorg Med Chem 16:6489–6500
11. Massi P, Vaccani A, Ceruti S, Colombo A, Abbracchio MP, Parolaro D (2004) Antitumor effects of cannabidiol, a nonpsychoactive cannabinoid, on human glioma cell lines. J Pharmacol Exp Ther 308(3):838–845
12. Sanchez C, de Ceballos ML, del Pulgar TG, Rueda D, Corbacho C, Velasco G, Galve-Roperh I, Huffman JW, Ramon y Cajal S, Guzman M (2001) Inhibition of glioma growth in vivo by selective activation of the CB(2) cannabinoid receptor. Cancer Res 61(15):5784–5789
13. Marcu JP, Christian RT, Lau D, Zielinski AJ, Horowitz MP, Lee J, Pakdel A, Allison J, Limbad C, Moore DH, Yount GL, Desprez PY, McAlliste rSD (2010) Cannabidiol enhances the inhibitory effects of delta9-tetrahydrocannabinol on human glioblastoma cell proliferation and survival. Mol Cancer Ther 9:180–189
14. Eichele K, Weinzierl U, Ramer R, Brune K, Hinz B (2006) R(+)-methanandamide elicits a cyclooxygenase-2-dependent mitochondrial apoptosis signaling pathway in human neuroglioma cells. Pharm Res 23:90–94
15. Blázquez C, González-Feria L, Alvarez L, Haro A, Casanova ML, Guzmán M (2004) Cannabinoids inhibit the vascular endothelial growth factor pathway in gliomas. Cancer Res 64:5617–5623
16. Blázquez C, Salazar M, Carracedo A, Lorente M, Egia A, González-Feria L, Haro A, Velasco G, Guzmán M (2008) Cannabinoids inhibit glioma cell invasion by down-regulating matrix metalloproteinase-2 expression. Cancer Res 68:1945–1952
17. Carracedo A, Lorente M, Egia A, Blázquez C, García S, Giroux V, Malicet C, Villuendas R, Gironella M, González-Feria L, Piris MA, Iovanna JL, Guzmán M, Velasco G (2006) The stress-regulated protein p8 mediates cannabinoid-induced apoptosis of tumor cells. Cancer Cell 9:301–312
18. Galve-Roperh I, Sanchez C, Cortes ML, del Pulgar TG, Izquierdo M, Guzman M (2000) Anti-tumoral action of cannabinoids: involvement of sustained ceramide accumulation and extracellular signal-regulated kinase activation. Nat Med 6(3):313–319
19. Salazar M, Carracedo A, Salanueva IJ, Hernández-Tiedra S, Lorente M, Egia A, Vázquez P, Blázquez C, Torres S, García S, Nowak J, Fimia GM, Piacentin iM, Cecconi F, Pandolf iPP, González-Feria L, Iovanna JL, Guzmán M, Boya P, Velasco G (2009) Cannabinoid action induces autophagy-mediated cell death through stimulation of ER stress in human glioma cells. J Clin Invest 119:1359–1372
20. Lorente M, Torres S, Salazar M, Carracedo A, Hernández-Tiedra S, Rodríguez-Fornés F, García-Taboada E, Meléndez B, Mollejo M, Campos-Martín Y, Lakatosh SA, Barcia J, Guzmán M, Velasco G (2011) Stimulation of the midkine/ALK axis renders glioma cells resistant to cannabinoid antitumoral action. Cell Death Differ 18:959–973
21. Galanti G, Fisher T, Kventsel I, Shoham J, Gallily R, Mechoulam R, Lavie G, Amariglio N, Rechavi G, Toren A (2008) Delta 9-tetrahydrocannabinol inhibits cell cycle progression by down-regulation of E2F1 in human glioblastoma multiforme cells. Acta Oncol 47:1062–1070
22. Guzmán M, Duarte MJ, Blázquez C, Ravina J, Rosa MC, Galve-Roperh I, Sánchez C, Velasco G, González-Feria L (2006) A pilot clinical study of Delta9-tetrahydrocannabinol in patients with recurrent glioblastoma multiforme. Br J Cancer 95:197–203
23. Ellert-Miklaszewska A, Grajkowska W, Gabrusiewicz K, Kaminska B, Konarska L (2007) Distinctive pattern of cannabinoid receptor type II (CB2) expression in adult and pediatric brain tumors. Brain Res 1137:161–169
24. De Jesús ML, Hostalot C, Garibi JM, Sallés J, Meana JJ, Callado LF (2010) Opposite changes in cannabinoid CB1 and CB2 receptor expression in human gliomas. Neurochem Int 56:829–833
25. Grotenhermen F (2003) Pharmacokinetics and pharmacodynamics of cannabinoids. Clin Pharmacokinet 42:327–360
26. Friedman HS, Colvin OM, Skapek SX, Ludeman SM, Elion GB, Schold SC Jr, Jacobsen PF, Muhlbaier LH, Bigner DD (1988) Experimental chemotherapy of human medulloblastoma cell lines and transplantable xenografts with bifunctional alkylating agents. Cancer Res 48(15):4189–4195

27. Friedman HS, Colvin OM, Skapek SX, Ludeman SM, Elion GB, Schold SCJ, Jacobsen PF, Muhlbaier LH, Bigner DD (1988) Experimental chemotherapy of human medulloblastoma cell lines and transplantable xenografts with bifunctional alkylating agents. Cancer Res 48:4189–4195

28. Gehan EAA (1965) Generalized wilcoxon test for comparing arbitrarily singly-censored samples. Biometrika 52:203–223

29. Gowan SM, Hardcastle A, Hallsworth AE, Valenti MR, Hunter LJ, de Haven Brandon AK, Garrett MD, Raynaud F, Workman P, Aherne W, Eccles SA (2007) Application of meso scale technology for the measurement of phosphoproteins in human tumor xenografts. Assay Drug Dev Technol 5:391–401

30. Eccles SA, Massey A, Raynaud FI, Sharp SY, Box G, Valenti M, Patterson L, de Haven Brandon A, Gowan S, Boxall F, Aherne W, Rowlands M, Hayes A, Martins V, Urban F, Boxall K, Prodromou C, Pearl L, James K, Matthews TP, Cheung KM, Kalusa A, Jones K, McDonald E, Barril X, Brough PA, Cansfield JE, Dymock B, Drysdale MJ, Finch H, Howes R, Hubbard RE, Surgenor A, Webb P, Wood M, Wright L, Workman P (2008) NVP-AUY922: a novel heat shock protein 90 inhibitor active against xenograft tumor growth, angiogenesis, and metastasis. Cancer Res 68:2850–2860

31. Koul D (2008) PTEN signaling pathways in glioblastoma. Cancer Biol Ther 7:1321–1325

32. Steck PA, Pershouse MA, Jasser SA, Yung WK, Lin H, Ligon AH, Langford LA, Baumgard ML, Hattier T, Davis T, Frye C, Hu R, Swedlund B, Teng DH, Tavtigian SV (1997) Identification of a candidate tumour suppressor gene, MMAC1, at chromosome 10q23.3 that is mutated in multiple advanced cancers. Nat Genet 15:356–362

33. Sun MG, Williams J, Munoz-Pinedo C, Perkins GA, Brown JM, Ellisman MH, Green DR, Frey TG (2007) Correlated three-dimensional light and electron microscopy reveals transformation of mitochondria during apoptosis. Nat Cell Biol 9:1057–1065

34. Jacobs VL, Valdes PA, Hickey WF, De Leo JA (2011) Current review of in vivo GBM rodent models: emphasis on the CNS-1 tumour model. ASN Neuro 3:171–181

35. Green DR, Reed JC (1998) Mitochondria and apoptosis. Science 281:1309–1312

36. Thornberry NA, Lazebnik Y (1998) Caspases: enemies within. Science 281:1312–1316

37. Ellert-Miklaszewska A, Kaminska B, Konarska L (2005) Cannabinoids down-regulate PI3K/Akt and Erk signalling pathways and activate proapoptotic function of Bad protein. Cell Signal 17:25–37

38. Greenhough A, Patsos HA, Williams AC, Paraskeva C (2007) The cannabinoid delta(9)-tetrahydrocannabinol inhibits RAS-MAPK and PI3K-AKT survival signalling and induces BAD-mediated apoptosis in colorectal cancer cells. Int J Cancer 121: 2172–2180

39. Jia W, Hegde VL, Singh NP, Sisco D, Grant S, Nagarkatti M, Nagarkatti PS (2006) Delta9-tetrahydrocannabinol-induced apoptosis in Jurkat leukemia T cells is regulated by translocation of Bad to mitochondria. Mol Cancer Res 4:549–562

40. Cudaback E, Marrs W, Moeller T, Stella N (2010) The expression level of CB1 and CB2 receptors determines their efficacy at inducing apoptosis in astrocytomas. PLoS ONE 5(1):e8702

41. Cattaneo E, Magrassi L, De-Fraja C, Conti L, Di Gennaro I, Butti G, Govoni S (1998) Variations in the levels of the JAK/STAT and ShcA proteins in human brain tumors. Anticancer Res 18:2381–2387

42. Caldera V, Mellai M, Annovazzi L, Valente G, Tessitore L, Schiffer D (2008) Stat3 expression and its correlation with proliferation and apoptosis/autophagy in gliomas. J Oncol Article ID 219241

43. Mizoguchi M, Betensky RA, Batchelor TT, Bernay DC, Louis DN, Nutt CL (2006) Activation of STAT3, MAPK, and AKT in malignant astrocytic gliomas: correlation with EGFR status, tumor grade, and survival. J Neuropathol Exp Neurol 65: 1181–1188

44. Liu Y, Li C, Lin J (2010) STAT3 as a therapeutic target for glioblastoma. Anticancer Agents Med Chem 10:512–519